Novel 1p tumour suppressor Dnmt1-associated protein 1 regulates MYCN/ataxia telangiectasia mutated/p53 pathway	Yamaguchi Y, Takenobu H, Ohira M, Nakazawa A, Yoshida S, Akita N, Shimozato O, Iwama A, Nakagawara A, Kamijo T	European Journal of Cancer	2014年	国外
Two Cases of Neuroblastoma Comprising Two Distinct Clones	Yamazaki F, Nakazawa A, Osumi T, Shimojima N, Tanaka T, Nakagawara A, Shimada H	Pediatric Blood Cancer	2014年	国外
RASSF1A methylation may have two biological roles in neuroblastoma tumorigenesis depending on the ploidy status and age of patients	Haruta M, Kamijo T, Nakagawara A, Kaneko Y	Cancer Letters	2014年	国外
Flotillin-1 regulates oncogenic signaling in neuroblastoma cells by regulating ALK membrane association	Tomiyama A, Uekita T, Kamata R, Sasaki K, Takita J, Ohira M, Nakagawara A, Kitanaka C, Mori K, Yamaguchi H, Sakai R	Cancer Research	2014年	国外
RUNX3 interacts with MYCN and facilitates protein degradation in neuroblastoma	Yu F, Gao W, Yokochi T, Suenaga Y, Ando K, Ohira M, Nakamura Y, Nakagawara A.	Oncogene	2014年	国外
Metastatic neuroblastoma confined to distant lymph nodes (stage 4N) predeicts outcome in patients with stage 4 disease: A study from the International Neuroblastoma Risk Group Database	Morgenstern DA, London WA, Stephens D, Volchenboum S, Hero B, Cataldo AD, Nakagawara A, Shimada H, Ambros P, Matthay KK, Cohn SL, Peason ADJ, Irwin MS.	Journal of Clinical Oncology	2014年	国外
Significance of clinical and biologic features in stage 3 neuroblastoma: A report from the International Neuroblastoma Risk Group project	Meany HJ, London WB, Ambros PF, Matthay KK, Monclair T, Simon T, Garaventa A, Berthold F, Nakagawara A, Cohn SL, Peason ADJ, Park JR.	Pediatric Blood & Cancer	2014年	国外
Clinical, biological, and prognostic differences on the basis of primary tumor site in neuroblastoma: a report from the international neuroblastoma risk group project	Vo KT, Matthay KK, Neuhaus J, London WB, Hero B, Ambros PF, Nakagawara A, Miniati D, Wheeler K, Pearson ADJ, Cohn SL, DuBois SG.	Journal of Clinical Oncology	2014年	国外
Revised risk estimation and treatment stratification of low- and intermediate-risk neuroblastoma patients by integrating clinical and molecular prognostic markers	Oberthuer A, Juraeva D, Hero B, Volland R, Carolina S, Schmidt R, Faldum A, Kahlert Y, Engesser A, Asgharzadeh S, Seeger RC, Ohira M, Nakagawara A, Scaruffi P, Tonini GP, Janoueix-Lerosey I, Delattre O, Schleiermacher G, Vandesompele J, Speleman F, Noguera R, Piqueras M, Benard J, Valent A, Avigad S, Yaniv I, Grundy RG, Ortmann M, Shao C, Schwab M, Eils R, Simon T, Theissen J, Berthold F, Westermann F, Brors B, Fischer M.	Clinical Cancer Research	2014年	国外
肝芽腫の診断と治療	上條岳彦、檜山英三	「最新肝癌学」、日本臨牀社	2014年	国内
Social and biological factors influencing the outcomes of children with Wilms tumors in Kenya and other Sub-Saharan countries	Kumon K, Kaneko Y.	Transl Pediatr	2014年	国外

Bilateral Wilms tumors treated according to the Japan Wilms Tumor Study Group protocol	Oue T, Koshinaga T, Okita H, Kaneko Y, Hinotsu S, Fukuzawa M.	Pediatr Blood Cancer	2014年	国外
Trim32 facilitates degradation of MYCN on spindle poles and induces asymmetric cell division in human neuroblastoma cells	Izumi H, Kaneko Y.	Cancer Research	2014年	国外
Wilms腫瘍(腎芽腫)の発生に関わるジェネティック・エピジェネティック異常、および遺伝性・両側性Wilms腫瘍の原因遺伝子	金子安比古	日本小児血液がん学会雑誌	2014年	国内
BMCC1, which is an interacting partner of BCL2, attenuates AKT activity, accompanied by apoptosis	Tatsumi Y, Takano R, Islam MS, Yokochi T, Itami M, Nakamura Y, Nakagawara A.	Cell Death and Disease	2015年	国外
Wilms腫瘍(腎芽腫)の分子生物学	金子安比古	小児外科	2015年	国内
A high incidence of *WT1* abnormality in bilateral Wilms tumours in Japan and children with *WT1* incidences of epigenetic but not genetic abnormalities germline mutation	Kaneko Y, Okita H, Haruta M, Arai Y, Oue T, Tanaka Y, Horie H, Hinotsu S, Koshinaga T, Yoneda A, Ohtsuka Y, Taguchi T, Fukuzawa M.	British Journal of Cancer	in press	国外

Ⅳ．研究成果の刊行物・別刷

Review Article

Pediatric hepatoblastoma: diagnosis and treatment

Eiso Hiyama

Department of Pediatric Surgery, Hiroshima University Hospital; and the Natural Science Center for Basic Research and Development (N-BARD), Hiroshima University, Hiroshima, Japan

Correspondence to: Eiso Hiyama, MD, PhD. Natural Science Center for Basic Research and Development, Hiroshima University, 1-2-3, Kasumi, Minami-ku, Hiroshima, 734-8551, Japan. Email: eiso@hiroshima-u.ac.jp.

Abstract: Hepatoblastoma (HBL) is the most common primary liver tumor in children, and is usually diagnosed during the first 3 years of life. Collaborative multicenter studies have led to improved diagnostic and treatment strategies. The pretreatment extent of disease (PRETEXT) staging system has become a consensus classification, and an international pathological classification system has also been developed. Clinical trials examining multimodal therapy, which consists of complete surgical resection plus liver transplantation and chemotherapy, have led to improved outcomes for children with HBL. Recently, the Children's Hepatic Tumors International Collaboration (CHIC), which includes major multicenter study groups, created a shared database that merges data on all children underwent therapy in the clinical trials of these groups until 2008. CHIC has developed a global approach to risk stratification of pediatric HBL for use in future global clinical trials. The aim of this review is to report the recent developments on the diagnosis and treatment of pediatric HBL.

Keywords: Hepatoblastoma (HBL); diagnosis; treatment; risk stratification; clinical trial

Submitted Jun 18, 2014. Accepted for publication Sep 24, 2014.
doi: 10.3978/j.issn.2224-4336.2014.09.01
View this article at: http://dx.doi.org/10.3978/j.issn.2224-4336.2014.09.01

Introduction

Hepatoblastoma (HBL) is the most common primary liver tumor in children and is usually diagnosed during the first 3 years of life. Most HBLs are sporadic, but some are associated with constitutional genetic abnormalities and malformations, such as the Beckwith-Wiedemann syndrome and familial adenomatous polyposis (1,2). Over the last three decades, the annual incidence of HBL in children has gradually increased (3). Extremely premature babies with a birth weight of less than 1 kilo have been reported to have a greatly increased risk of developing HBL. The increased survival rates of these premature babies might account for the increased annual incidence of HBL.

Diagnosis of HBL

The most common sign is abdominal distension or abdominal mass. Some children present with abdominal discomfort, generalized fatigue, and loss of appetite, due to tumor distension or secondary anemia. Children with a ruptured tumor usually present with vomiting, symptoms of peritoneal irritation, and severe anemia. Rare cases manifest precocious puberty/virilization due to β-human chorionic gonadotropin (hCG) secretion by the tumor. Serum alpha-fetoprotein (AFP) is the most important clinical marker for HBL, and remains the key clinical marker of malignant change, response to the treatment, and relapse. However, there are some variants of both HBL and hepatocellular carcinoma (HCC) that have low or normal AFP levels (4,5). These variants, such as rhabdoid tumor, may have distinct histological features and worse prognosis.

Abdominal ultrasonography usually reveals a large mass in liver, sometimes with satellite lesions and areas of hemorrhage within the tumor. The most useful diagnostic modality is multiphase computed tomography (CT) or magnetic resonance imaging (MRI). Helical CT findings of hypervascular lesions in the liver with delayed contrast excretion are highly suggestive of a malignant liver tumor. Histological diagnosis of a tumor specimen is essential,

Table 1 CHIC proposed—Hepatoblastoma Risk Stratification (CHICS)

PRETEXT	Standard risk (SR)		High risk (HR)	Very high risk (VHR)
	Low risk (LR) (primary resection at diagnosis)	Intermediate risk (IR)		
Any M+	–	–	–	M+
I M–	VPERF—(any AFP, any age)	–	VPERF + AND age <8 years (any AFP)	VPERF + AND age ≥8 years
II M–	VPERF—AND Age <3 AND AFP >1,000 ng/mL	VPERF—AND Age <3 AND AFP 100-1,000 ng/mL	Age 3-7 AND/OR VPERF +	AFP <100 ng/mL, AND/OR age ≥8 years
III M–	–	VPERF—AND Age<3 AND AFP >1,000 ng/mL	Age 3-7 AND/OR VPERF + AND/OR AFP 100-1,000 ng/mL	AFP <100 ng/mL, AND/OR age ≥8 years
IV M–	–	–	AFP >100 ng/mL	AFP <100 ng/mL, AND/OR age ≥8 years

M+, distant metastases; VEPRF+, one or more of the following criteria; V, hepatic vein/cava involvement; P, portal vein involvement; E, contiguous extrahepatic tumor; R, rupture at diagnosis; F, multifocality; AFP, α-fetoprotein (ng/mL); PRETEXT, pretreatment extent of disease.

although some investigators believe that biopsy may not be necessary for young children (6 months to 3 years) with a very high AFP level (6); in addition, avoiding a biopsy theoretically reduces the risks of tumor seeding or dissemination. The Japanese Study Group for Pediatric Liver Tumors (JPLT) strongly recommends that liver tumors of children should be treated after definitive diagnosis of a biopsy specimen, except in urgent life-threatening circumstances such as tumor invasion of the right atrium or tumor rupture (7).

Segmental assessment of the extent of the tumor and its relationship to the main hepatic vessels is of utmost importance when planning the intensity of chemotherapy and eventual surgery. In Europe, the Childhood Liver Tumor Study Group of the International Society of Pediatric Oncology (SIOPEL) has developed the preoperative evaluation of the tumor extent (PRETEXT) staging system, which appears to be a valuable tool for risk stratification (8); although the system has not been formally evaluated for prognostic accuracy. Formal staging of the tumor should include chest and brain CT. The risk stratification system proposed by the Children's Hepatic Tumors International Collaboration (CHIC), which will be described later, is shown in *Table 1*.

In childhood hepatic tumors, clinically relevant histologic subtypes are also being incorporated into risk stratification systems as well as into the PRETEXT staging system and distant metastasis. The common HBL subtypes are as follows: epithelial, mesenchymal, fetal, and embryonal. Some HBL variants include cholangioblastic or teratoid components or a macrotrabecular growth pattern (9). Fibrolamellar HCC is a distinct clinical and histological variant of pediatric HCC. The histopathological subtypes are the major prognostic factors of pediatric liver tumors, including HCC. The Children's Oncology Group (COG) has found that patients with completely resected tumors (stage I) with pure fetal histology have an excellent outcome (10), while both the SIOPEL and the COG investigators found that HBL patients presenting with low AFP levels (<100 ng/mL) and/or with small cell undifferentiated (SCUD) histology had a poor outcome, regardless of the PRETEXT staging system (4,5). The SCUD histology has not been reported by Japanese investigators. Rhabdoid tumors, which show loss of SMARCB1/INI1 expression on immunohistochemistry, should be included in the differential diagnosis of patients with tumors and low AFP levels (11). In 2011, an International Pathology Symposium was held to perform a collaborative histopathological review of pediatric liver tumors to work towards a consensus classification, with the eventual aim of developing a common treatment-stratification system. This symposium proposed the current standardized, histopathological meaningful classification of pediatric liver tumors (12).

Treatments for HBL

Before 1980, children with malignant hepatic tumors could only be cured by complete surgical resection of tumors. At present, complete tumor resection remains the cornerstone of definitive cure for HBL and offers the only realistic chance of long-term disease-free survival (13-15). The introduction of effective chemotherapeutic regimens in the 1980s resulted in an increased number of patients who could ultimately undergo tumor resection and also reduced the postoperative recurrence rate. Moreover, modern surgical techniques based on the segmental anatomy of the liver and whole hepatectomy plus liver transplantation have also led to increased numbers of resectable patients and have markedly improved the prognosis of these patients. Therefore, the combination of surgery and chemotherapy is an essential therapeutic strategy for HBL. The COG and JPLT studies have approved primary resection for children with resectable tumors, especially PRETEXT I or II cases. However, SIOPEL studies have not permitted the used of primary resection.

Recently, international collaboration study should be required for prompt clinical trials. CHIC was formed to focus on international global cooperation for investigations of pediatric malignant hepatic tumors, including HBL. The leading multicenter groups in CHIC are JPLT, SIOPEL, GPOH (German Paediatric Oncology and Haematology Society) and COG. Risk stratification in these trials was based on individual special classification of stage, metastasis, and histology in each trial (16). These CHIC members have incorporated their unique data into a common database, which now includes the retrospective data of all children treated in eight separate multicenter HBL trials performed between 1985 and 2008 (1,605 patients) (13-15,17-23).

The identification and development of new prognostic stratifications has led to novel treatments for high-risk patients and treatment reduction for low-risk patients, who do not need therapy intensification but need to avoid the delayed effects and unnecessary toxicities associated with treatment (24). Since childhood cancers are leading the way in the use of risk-adapted therapeutic strategies (25,26), collaborative research based on common risk adaptations and chemoprotective therapy for toxicity will have many benefits throughout the field of pediatric oncology. Although the analysis of CHIC database is still being debated, the therapeutic strategies used in global studies will be proposed using the risk stratification system proposed by CHIC (*Table 1*).

Standard-/low-risk patients

Patients with a single localized tumor involving at most three segments of the liver (PRETEXT I, II, III) can safely undergo complete surgical resection because of recently developed surgical instruments and anatomical evaluation using imaging modalities. Standard-risk patients are those patients with PRETEXT I, II, and III tumors and no extrahepatic features [hepatic vein/cava involvement (V), portal vein involvement (P), contiguous extrahepatic tumor (E), rupture at diagnosis (R), and multifocality (F)] or distant metastasis (M) (*Table 1*).

The treatment algorithm is shown in *Figure 1*. JPLT and COG have permitted primary hepatectomy for patients with PRETEXT I and II tumors, but SIOPEL has recommended preoperative chemotherapy for every patient, which is followed by tumor resection (19,27-29) or liver transplantation (27), and a short course of postoperative chemotherapy for most cases. The current consensus based on CIHC analysis is that an initial resection can be performed for PRETEXT I or II tumors if the tumor is located at least 1 cm from the middle hepatic vein and the bifurcation of the portal vein. Preoperative chemotherapy should be performed for other situations. Cisplatin-and-anthracycline-based chemotherapy was used as the first-line regimen in European (SIOPEL) and Japanese (JPLT) studies. This regimen improved the survival rates of patients with resectable tumors (15,17). The SIOPEL-1 study (PLADO) used four triweekly preoperative and two postoperative cycles of cisplatin (CDDP) and doxorubicin (DOXO), and resulted in an overall response rate of 82% and 5-year event-free survival (EFS) of 66% (28). The JPLT studies, using the same four preoperative and two postoperative cycles of CDDP and pirarubicin (THP-ADM), and the COG studies, using the same cycles of CDDP, fluorouracil (5-FU), and vincristine, resulted in almost similar survival rates. CDDP monotherapy recently achieved similar rates of complete resection and survival among children with resectable tumors (15). Therefore, CDDP monotherapy will be first-line chemotherapy for these standard HBLs. A trial is underway that evaluates combination therapy using CDDP and sodium thiosulphate to reduce the late effects of CDDP, especially ototoxicity.

High-risk (HR) patients

These patients are those with unresectable tumor at diagnosis and/or associated with so-called "combi

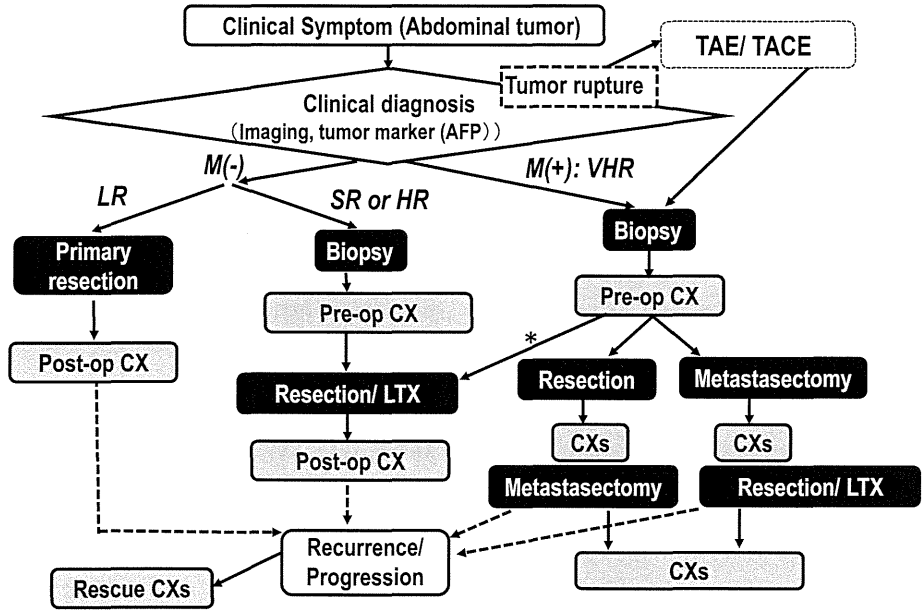

Figure 1 Diagnosis and treatment algorithm for hepatoblastoma. Hepatoblastoma is usually diagnosed from clinical signs, imaging findings, and elevation of serum α-fetoprotein (AFP) levels. In some patients whose tumor is ruptured, transarterial embolization (TAE) or transarterial chemoembolization (TACE) is needed for control of intraperitoneal bleeding. After bleeding is controlled, these patients should be treated according to the following risk stratification. Among the patients without distant metastasis [M(-)], low-risk (LR) patients are treated by primary resection followed by postoperative chemotherapy (Post-op CX). Standard-risk (SR) [intermediate-risk (IR) in *Table 1*] or high-risk (HR) patients receive preoperative chemotherapy (Pre-op CX) and then undergo primary tumor resection by hepatectomy or liver transplantation (LTX). The very high-risk (VHR) patients with distant metastasis [M(+)] receive Pre-op CX. Then, a patient whose distant metastasis is diminished by CX undergoes primary tumor resection by hepatectomy or LTX followed by Post-op CX; a patient whose distant metastasis remains undergoes metastasectomy or hepatectomy. LTX is usually indicated for the patient without distant metastasis or whose distant metastasis has clearly disappeared. Patients with recurrence or tumor progression should undergo rescue chemotherapy. Consolidation therapy has not been established as additional treatment for these HR and VHR patients who have undergone these multimodal therapies.

factors" without distant metastasis. The combi factor is a combination of the cross sectional imaging components including macrovascular involvement retrohepatic vena cava or all three hepatic veins (V); macrovascular involvement portal bifurcation or both right and left portal veins (P); contiguous extrahepatic tumor (E); multifocal disease (F); and spontaneous rupture (R) at diagnosis. V, P, E, F and R where a patient is categorized as positive when at least 1 of the components is present in HR. In addition, CHIC analysis found that older patients (≥3 years old at diagnosis) and patients with ruptured or multifocal tumors at diagnosis had unfavorable outcomes. Therefore, these patients were included as high-risk patients, even if their tumor was resectable (30,31). Conventional preoperative chemotherapy used in the PLADO, CITA, and C5V trials for patients with PRETEXT IV unresectable tumors resulted in tumors that could be resected by hepatectomy in some patients; but the outcome of patients with unresectable tumors at diagnosis remained unsatisfactory. Therefore, in SIOEPL studies, chemotherapy for HR-HBL was gradually intensified by the addition of carboplatin (SuperPLADO study) or high-dose CDDP (SIOPEL-4 study) with shortened intervals between chemotherapy cycles (31,32). In COG studies, the HR-HBL regimen was also intensified by addition of DOXO and high-dose CDDP (C5VD) (33). The SIOPEL-4 and COG approaches, based on CDDP intensification, improved the survival of children with HR-HBL, including those with lung metastases. Therefore, at present, CDDP intensification protocols are being evaluated for patients with HR-HBL, although the toxicity and late complications of these treatment protocols remain unclear.

In addition, orthotropic liver transplantation has

improved the outcome for some patients with unresectable tumors (PRETEXT IV tumors or tumors with portal or hepatic vein involvement) (34). Although the timing of liver transplantation and the role of rescue transplantation therapy remain controversial, consultation for liver transplantation should be performed for high-risk patients during the early stages of preoperative chemotherapy.

Very high-risk patients (metastatic HBL)

There is strong agreement that patients who present with lung metastases have a poor prognosis. In addition, CHIC analysis revealed that older patients (≥8 years old at diagnosis) and patients with low AFP levels (<100 ng/mL) have unfavorable outcomes. Therefore, these patients were included as very high-risk patients even if their tumor had not metastasized (35,36).

Conventional chemotherapy was usually ineffective for these very high-risk patients, with survival rates under 40% in the previous SIOPEL-1 and JPLT-1 studies (8,18). Moreover, resection of lung metastases has been effective for some patients with metastatic tumors. The surgical guideline for lung metasectomy should be necessary to improve outcome of the patient with lung metastasis in future. CDDP intensification therapy such as that used in the SIOPEL-4 protocol seems to be effective for these patients. The 3-year survival of metastatic HBL cases who underwent the SIOPEL-4 protocol was approximately 80% (31). To decrease recurrence, a consolidation regimen should be considered for these very high-risk patients. In addition, new molecular targeting therapy using vincristine and irinotecan will be investigated by COG.

For some of these metastatic patients whose metastatic lesions respond to these approaches, liver transplantation may be an indication. Therefore, carefully planned combination therapy using dose-intensified chemotherapy and surgical approaches that include metastasectomy and liver transplantation should be required to treat the very high-risk HBL patient.

Other therapies

Transarterial embolization (TAE) is used to control peritoneal hemorrhage in patients with ruptured tumors. Since primary resection for such rupture cases results in poor outcome, interventional control for hemorrhage is required for more successful treatment of these HBL patients.

It is well known that the normal liver receives blood from two sources, the hepatic artery and portal vein. Malignant liver tumors, including HBL, are mainly fed by the hepatic artery. Therefore, transarterial chemoembolization (TACE) is tumor selective. JPLT has used TACE instead of systemic chemotherapy as a clinical trial (17). CDDP and anthracycline have infused with particles that are used for embolization. The effect of TACE for HBL seemed to be equivalent to that of the patients who were treated by systemic chemotherapy and might be less toxic in comparison with systemic chemotherapy. Therefore, TACE is one of the effective procedures for pediatric liver tumors. However, administering TACE to children is somewhat difficult and requires general anesthesia. Verification of the efficacy of TACE for patients with standard-risk HBL requires additional clinical trials.

Future plans

To obtain consensus for universal risk stratification and treatment of pediatric HBL, CHIC has created the largest database to date of patients with this rare cancer. The CHIC based classification system described in this review is being incorporated into a new risk-based cooperative international trial, the Pediatric Hepatoblastoma International Therapeutic Trial (PHITT), a joint venture of global collaboration that includes SIOPEL, COG, and JPLT.

Acknowledgements

This review was partially supported by Grants-in-Aid for Scientific Research (A) (No. 13313631 and 13370806) from the Ministry of Education, Culture, Sports, Science, and Technology and for Cancer Research by that from the Ministry of Health, Labor, and Welfare of the Government of Japan (No. H26-Kakushintekigun-Ippan-067, and H26-Iryougijyutu-Ippan-008).
Disclosure: The author declares no conflict of interest.

References

1. Cohen MM Jr. Beckwith-Wiedemann syndrome: historical, clinicopathological, and etiopathogenetic perspectives. Pediatr Dev Pathol 2005;8:287-304.
2. Garber JE, Li FP, Kingston JE, et al. Hepatoblastoma and familial adenomatous polyposis. J Natl Cancer Inst 1988;80:1626-8.
3. Linabery AM, Ross JA. Trends in childhood cancer incidence

in the U.S. (1992-2004). Cancer 2008;112:416-32.
4. De Ioris M, Brugieres L, Zimmermann A, et al. Hepatoblastoma with a low serum alpha-fetoprotein level at diagnosis: the SIOPEL group experience. Eur J Cancer 2008;44:545-50.
5. Trobaugh-Lotrario AD, Tomlinson GE, Finegold MJ, et al. Small cell undifferentiated variant of hepatoblastoma: adverse clinical and molecular features similar to rhabdoid tumors. Pediatr Blood Cancer 2009;52:328-34.
6. Czauderna P, Otte JB, Aronson DC, et al. Guidelines for surgical treatment of hepatoblastoma in the modern era--recommendations from the Childhood Liver Tumour Strategy Group of the International Society of Paediatric Oncology (SIOPEL). Eur J Cancer 2005;41:1031-6.
7. Nitta A, Hisamatsu S, Fukuda H, et al. Cardiopulmonary arrest on arrival in an infant due to ruptured hepatoblastoma. J Pediatr 2012;160:351.
8. Perilongo G, Shafford E, Plaschkes J, et al. SIOPEL trials using preoperative chemotherapy in hepatoblastoma. Lancet Oncol 2000;1:94-100.
9. López-Terrada D, Zimmermann A. Current issues and controversies in the classification of pediatric hepatocellular tumors. Pediatr Blood Cancer 2012;59:780-4.
10. Malogolowkin MH, Katzenstein HM, Meyers RL, et al. Complete surgical resection is curative for children with hepatoblastoma with pure fetal histology: a report from the Children's Oncology Group. J Clin Oncol 2011;29:3301-6.
11. Al Nassan A, Sughayer M, Matalka I, et al. INI1 (BAF 47) immunohistochemistry is an essential diagnostic tool for children with hepatic tumors and low alpha fetoprotein. J Pediatr Hematol Oncol 2010;32:e79-81.
12. López-Terrada D, Alaggio R, de Dávila MT, et al. Towards an international pediatric liver tumor consensus classification: proceedings of the Los Angeles COG liver tumors symposium. Mod Pathol 2014;27:472-91.
13. Ortega JA, Douglass EC, Feusner JH, et al. Randomized comparison of cisplatin/vincristine/fluorouracil and cisplatin/continuous infusion doxorubicin for treatment of pediatric hepatoblastoma: A report from the Children's Cancer Group and the Pediatric Oncology Group. J Clin Oncol 2000;18:2665-75.
14. Pritchard J, Brown J, Shafford E, et al. Cisplatin, doxorubicin, and delayed surgery for childhood hepatoblastoma: a successful approach--results of the first prospective study of the International Society of Pediatric Oncology. J Clin Oncol 2000;18:3819-28.
15. Perilongo G, Maibach R, Shafford E, et al. Cisplatin versus cisplatin plus doxorubicin for standard-risk hepatoblastoma. N Engl J Med 2009;361:1662-70.
16. Le Bail B. Pathology: a pictorial review. A selected atlas of paediatric liver pathology. Clin Res Hepatol Gastroenterol 2012;36:248-52.
17. Hishiki T, Matsunaga T, Sasaki F, et al. Outcome of hepatoblastomas treated using the Japanese Study Group for Pediatric Liver Tumor (JPLT) protocol-2: report from the JPLT. Pediatr Surg Int 2011;27:1-8.
18. Sasaki F, Matsunaga T, Iwafuchi M, et al. Outcome of hepatoblastoma treated with the JPLT-1 (Japanese Study Group for Pediatric Liver Tumor) Protocol-1: A report from the Japanese Study Group for Pediatric Liver Tumor. J Pediatr Surg 2002;37:851-6.
19. Perilongo G, Shafford E, Maibach R, et al. Risk-adapted treatment for childhood hepatoblastoma. final report of the second study of the International Society of Paediatric Oncology--SIOPEL 2. Eur J Cancer 2004;40:411-21.
20. Fuchs J, Rydzynski J, Von Schweinitz D, et al. Pretreatment prognostic factors and treatment results in children with hepatoblastoma: a report from the German Cooperative Pediatric Liver Tumor Study HB 94. Cancer 2002;95:172-82.
21. Häberle B, Bode U, von Schweinitz D. Differentiated treatment protocols for high- and standard-risk hepatoblastoma--an interim report of the German Liver Tumor Study HB99. Klin Padiatr 2003;215:159-65.
22. Katzenstein HM, Rigsby C, Shaw PH, et al. Novel therapeutic approaches in the treatment of children with hepatoblastoma. J Pediatr Hematol Oncol 2002;24:751-5.
23. Katzenstein HM, Chang KW, Krailo M, et al. Amifostine does not prevent platinum-induced hearing loss associated with the treatment of children with hepatoblastoma: a report of the Intergroup Hepatoblastoma Study P9645 as a part of the Children's Oncology Group. Cancer 2009;115:5828-35.
24. McDermott U, Settleman J. Personalized cancer therapy with selective kinase inhibitors: an emerging paradigm in medical oncology. J Clin Oncol 2009;27:5650-9.
25. Walterhouse D, Watson A. Optimal management strategies for rhabdomyosarcoma in children. Paediatr Drugs 2007;9:391-400.
26. Gustafson WC, Matthay KK. Progress towards personalized therapeutics: biologic- and risk-directed therapy for neuroblastoma. Expert Rev Neurother 2011;11:1411-23.
27. Czauderna P. Hepatoblastoma throughout SIOPEL trials - clinical lessons learnt. Front Biosci (Elite Ed) 2012;4:470-9.
28. Perilongo G, Brown J, Shafford E, et al. Hepatoblastoma

presenting with lung metastases: treatment results of the first cooperative, prospective study of the International Society of Paediatric Oncology on childhood liver tumors. Cancer 2000;89:1845-53.
29. Perilongo G, Malogolowkin M, Feusner J. Hepatoblastoma clinical research: lessons learned and future challenges. Pediatr Blood Cancer 2012;59:818-21.
30. von Schweinitz D. Hepatoblastoma: recent developments in research and treatment. Semin Pediatr Surg 2012;21:21-30.
31. Zsiros J, Brugieres L, Brock P, et al. Dose-dense cisplatin-based chemotherapy and surgery for children with high-risk hepatoblastoma (SIOPEL-4): a prospective, single-arm, feasibility study. Lancet Oncol 2013;14:834-42.
32. Zsíros J, Maibach R, Shafford E, et al. Successful treatment of childhood high-risk hepatoblastoma with dose-intensive multiagent chemotherapy and surgery: final results of the SIOPEL-3HR study. J Clin Oncol 2010;28:2584-90.
33. Meyers RL, Tiao G, de Ville de Goyet J, et al. Hepatoblastoma state of the art: pre-treatment extent of disease, surgical resection guidelines and the role of liver transplantation. Curr Opin Pediatr 2014;26:29-36.
34. Meyers RL, Tiao GM, Dunn SP, et al. Liver transplantation in the management of unresectable hepatoblastoma in children. Front Biosci (Elite Ed) 2012;4:1293-302.
35. Czauderna P, Lopez-Terrada D, Hiyama E, et al. Hepatoblastoma state of the art: pathology, genetics, risk stratification, and chemotherapy. Curr Opin Pediatr 2014;26:19-28.
36. Watanabe K. Current chemotherapeutic approaches for hepatoblastoma. Int J Clin Oncol 2013;18:955-61.

Cite this article as: Hiyama E. Pediatric hepatoblastoma: diagnosis and treatment. Transl Pediatr 2014;3(4):293-299. doi: 10.3978/j.issn.2224-4336.2014.09.01

Journal of Pediatric Surgery 49 (2014) 1835–1838

Contents lists available at ScienceDirect

Journal of Pediatric Surgery

journal homepage: www.elsevier.com/locate/jpedsurg

Clinical features of *ATRX* or *DAXX* mutated neuroblastoma

Sho Kurihara [a,b], Eiso Hiyama [a,b,c,*], Yoshiyuki Onitake [a,b], Emi Yamaoka [c], Keiko Hiyama [c]

[a] Graduate School of Biomedical Science & Health, Hiroshima University, Hiroshima 734-8551 Japan
[b] Department of Pediatric Surgery, Hiroshima University Hospital, Hiroshima 734-8551 Japan
[c] Natural Science Center for Basic Research and Development (N-BARD), Hiroshima University, Hiroshima, Japan

ARTICLE INFO

Article history:
Received 28 August 2014
Accepted 5 September 2014

Key words:
ATRX
DAXX
Neuroblastoma
Mutation
Telomere
ALT
Prognosis

ABSTRACT

Purpose: Previously, we reported that alternative lengthening of telomere (ALT) may be a biomarker for chemosensitivity and late recurrence in neuroblastoma (NBL). In this study, alterations of *ATRX* or *DAXX*, which both encode chromatin remodeling proteins in telomeric region, and their relationship to ALT were examined in NBLs.
Methods: Our previous report on 121 NBLs revealed 11 NBLs with elongated telomeres by ALT. In these NBLs, *ATRX* or *DAXX* gene alterations were identified using next-generation sequencing and compared to clinical and other biological factors.
Results: In 11 ALT cases, *DAXX* mutations were detected in one case, and *ATRX* alterations were detected in 10 cases. Except for one case, no *DAXX* or *ATRX* alterations were detected in 110 tumors with normal or shortened telomeres. *MYCN* amplification was not detected in *ATRX* altered tumors. In ALT cases, three infants showed *ATRX* deletions, and all seven cases detected after 18 months of age showed poor prognosis.
Conclusions: In NBLs, ALT was caused by *ATRX* or *DAXX* alterations. *ATRX* altered cases without *MYCN* amplification detected at greater than 18 months showed poor prognosis, suggesting that *ATRX* or *DAXX* alterations are a particular NBL subtype. Since these tumors showed chemo-resistance and late recurrence, complete resection in a surgical approach should be performed to improve patient prognosis.

More than 90% of neuroblastomas (NBLs) are diagnosed within the first five years of age and exhibit different clinical behaviors such as life-threatening progression, and spontaneous regression or maturation. Since most NBLs produce catecholamines, vanillylmandelic acid (VMA) and homovanillic acid (HVA) are detectable in urine. In Japan, mass-screening of catecholamine metabolites to detect earlier stage NBLs in infants showed that the annual incidence increased more than two-fold prior to screening implementation, whereas both incidence of advanced NBLs in older children and cumulative mortality rate of NBLs were reduced significantly [1]. Therefore, NBLs consist of heterogeneous subtypes and the unfavorable subtypes increase in the older children.

Molecular and biological analyses revealed several distinguishable NBL subtypes with alterations in *MYCN*, *ALK*, *PHOX2*, *PTPN11*, *ATRX*, and *NRAS*[2,3]. *MYCN* amplification and hemizygous deletions of chromosomes 1p and 11q are highly recurrent and associated with poor prognosis in NBLs [4]. Heritable mutations in *ALK* or *PHOX2B* account for the majority of familial NBLs [5,6]. One distinguishable NBL characteristic, ALT (Alternative Lengthening of Telomere), was associated with unfavorable NBLs in older children without *MYCN* amplification [7–9]. Cheung et al. found *ATRX* loss-of-function mutations and deletions associated with NBLs in adolescents and young adults [10]. In this paper, we focused on *ATRX* and *DRXX* alterations in association with ALT activated tumors.

1. Materials and methods

1.1. Samples

Approximately 500 NBL cases, whose tumors were obtained prior to any treatment, were diagnosed at Hiroshima University Hospital or affiliated hospitals in Japan over the past two decades. As shown in our previous study [9], 121 cases that were followed for more than 2 years and had high quality isolated DNA and RNA were selected for further study. Mean age at initial diagnosis was 22.2 months (range, 0-168 months). Among these cases, 67 were detected by mass-screening in Japan at 6 months of age [1]. Clinical stages and histological findings were determined according to the International Neuroblastoma Staging System (INSS) [11] and the International Neuroblastoma Pathological Classification (INPC) [12]. Written informed consent was obtained from all subjects or from their parents before surgery and this study was approved by the Institutional Review Board of Hiroshima University (I-RINRI-Hi-No.20). NBLs were routinely examined for *MYCN* amplification using fluorescent *in situ* hybridization or qualitative PCR analysis, and DNA ploidy using flow-cytometry analysis.

Patients of any age with INSS 1 or 2 disease, and those less than 12 months old with INSS 3 or 4S disease were treated with either surgery or both surgery and chemotherapy. Patients 12 months or older with INSS 3 and 4 disease were typically treated according to the

* Corresponding author at: Natural Science Center for Basic Research, Hiroshima University, 1-2-3, Kasumi, Minami-ku, Hiroshima, 734-8551, Japan. Tel.: +81 82 257 5951; fax: +81 82 257 5416.
E-mail address: eiso@hiroshima-u.ac.jp (E. Hiyama).

http://dx.doi.org/10.1016/j.jpedsurg.2014.09.029
0022-3468/

Japanese Neuroblastoma Study Group protocols [13]. In the cases with INSS 4 tumor or INSS 3 *MYCN* amplified tumor, most patients, except for some infants, underwent myeloablative chemotherapy followed by bone marrow transplantation.

1.2. Affymetrix platform

Array experiments were done according to standard protocols for Affymetrix GeneChip Mapping SNP 6.0 arrays (Affymetrix, Inc., Santa Clara, CA), which can detect genomic gains or deletions leading to LOH [14]. These arrays were scanned with the Affymetrix GeneChip Scanner 3000 using GeneChip Operating System 1.2 (Affymetrix). Genotype calls and intensity of the single nucleotide polymorphisms (SNP) were processed by GeneChip DNA Analysis Software. Individual SNP copy intensity and regions in the *ATRX* gene were evaluated with the Affymetrix Genotyping Console Workflow.

1.3. ATRX and DAXX mutation analysis

Target genes including *ATRX* and *DAXX* were chosen for next-generation sequencing. Primers for each gene were designed using DesignStudio (Illumina Inc., San Diego, CA). Using the Nextera Custom Enrichment system (Illumina), sample libraries were generated from 50 ng of DNA. Using a paired-end sequencing approach, 112 target genes were sequenced. Single nucleotide variations and deletions were identified using previously described methods [15].

To validate the identified *ATRX* and *DAXX* mutations by Sanger sequencing, PCR primers were designed for each exon of these genes according to previous reports [16] and each exon was amplified from genomic DNA using exon-specific primers. Sequencing products were purified using Centri-Sep Spin Columns (Princeton Separations, USA) and then prepared for analysis on the ABI 3100-Avant Genetic Analyzer (Applied Biosystems, USA) according to the manufacturer's instructions.

1.4. Telomere analysis

Telomere length was estimated as the length of terminal restriction fragments (TRFs) by Southern as previously described [17]. Briefly, genomic DNA was digested with *Hinf*I, separated by electrophoresis on 0.8% agarose, and hybridized with a 5'-end [^{32}P]-labeled $(TTAGGG)_4$ probe. Signal peaks were estimated as the TRF length. Length of 3'-overhang (3'-OH), single strand of the telomere end, was measured by a telomere-oligonucleotide ligation assay (T-OLA) [18,19]. Normalized 3'-OH intensity was then calculated in comparison with that of HeLa cells (defined as 1.0), which were run on each gel.

1.5. Quantification of telomerase activity

Extraction of telomerase protein and evaluation of activity were done by the TRAP (telomeric repeat amplification protocol) assay as described [20,21]. Levels of telomerase activity, expressed as Total Product Generated (TPG) units, were quantified by examining the ratio of the fluorescein intensity of the entire TRAP ladder. Since telomerase activity levels in fetal adrenal gland tissue were under 10.0 TPG, telomerase activity levels were divided into four categories: undetectable (TPG < 1.0), low (1.0 ≤ TPG < 10.0), moderate (10.0 ≤ TPG < 100.0), and high (TPG > 100.0).

1.6. Statistical analysis

Chi-square test or Mann–Whitney's U test was used to examine the significance of the comparisons of telomerase activity, telomere length, and clinicopathological factors. A log rank test was used to evaluate survival rates. Statistical significance was defined as $p < 0.05$.

2. Results

2.1. Single nucleotide polymorphism (SNP) analysis data using Affymetrix platform

SNP signals around *ATRX* and *DAXX* regions were analyzed by the SNP 6.0 array in 121 tumors including 11 tumors with elongated telomeres. Large deletions in *ATRX* were detected in 8 tumors (6.6%) (Fig. 1) and no deletions in *DAXX* were identified. The *ATRX*-deleted cases included 5 males and 3 females and 7 of these cases had elongated telomeres. The minimum overlapping deleted region contained exon 5 to exon 10, which encodes a predicted nuclear localization signal (Fig. 1).

2.2. ATRX and DAXX sequencing

We performed on discovery of the *ATRX* and *DAXX* gene alterations on the cohort of the remaining 114 cases without deleted *ATRX* gene using the next-generation sequencing and/or Sanger method. A *DAXX* mutation was detected in only one case with elongated telomere. This mutation results in a frame-shift of *DAXX* (A470 indel). *ATRX* mutations were also detected in three cases with elongated telomeres. Two were missense mutations (Q929E and A1690D) and the remaining one was a nonsense mutation (E555*). Neither *DAXX* nor *ATRX* mutations were detected in the cases without elongated telomeres.

2.3. Telomere length, 3'-OH length, and telomerase activity in NBLs

We previously reported no correlation between telomere length and telomerase activity, but did find a significant correlation between telomere length and 3'-OH length [10]. In this study, we identified *DAXX* or *ATRX* alterations (4 mutations and 7 deletions) in all NBLs with elongated telomeres (>15 kb) and a long length of 3'-OHs (>1.5). On the other hand, no alterations of *DAXX* or *ATRX* were detected in the remaining 110 cases, except for one case. Therefore, *DAXX* or *ATRX* alterations might contribute to ALT activation in NBLs. The *ATRX* deleted case without elongated telomeres also had elongated 3'-OH (Table 1).

2.4. Clinical and biological features of cases with ATRX and DAXX alterations

For patients detected either clinically or in large scale screens, clinical features of all cases with detected *ATRX* and *DAXX* mutations are shown in Table 1. Survival rate for patients with high telomerase activity had already been shown to be less than for those with other tumors ($P < 0.0001$) (Fig. 2) [9]. However, tumors without high telomerase activity did not usually show good prognosis. In this study, we analyzed the correlation between patient outcome and *ATRX* alterations of the tumor. Since high telomerase activity is well known as a poor prognostic marker, we analyzed prognosis of patients with tumors that did not have high telomerase activity (Fig. 2). The *ATRX* altered cases showed significantly worse prognosis.

Among the *ATRX or DAXX* altered cases, 8 INSS 4 tumors showed poor outcomes except for one infant case (Table 1). In these deceased cases, survival periods were more than 2 years and relatively long as compared with the deceased cases without *ATRX* or *DAXX* alterations. These cases with these aberrations, except for one, responded poorly to myeloablative chemotherapy. Moreover, the patient with complete remission also relapsed soon afterwards, and died of the disease. *ATRX* or *DAXX* altered NBLs diagnosed at older ages did not have high proliferative capacities, but showed poor outcomes due to chemoresistance. Although these alterations were very rare in tumors without elongated telomeres, one screening-detected case showed the *ATRX* deletion. Clinical feature of this *ATRX* deletion case without elongated telomeres included a ranking of INSS1, complete resection by surgery, but death by recurrence 25 months after initial diagnosis.

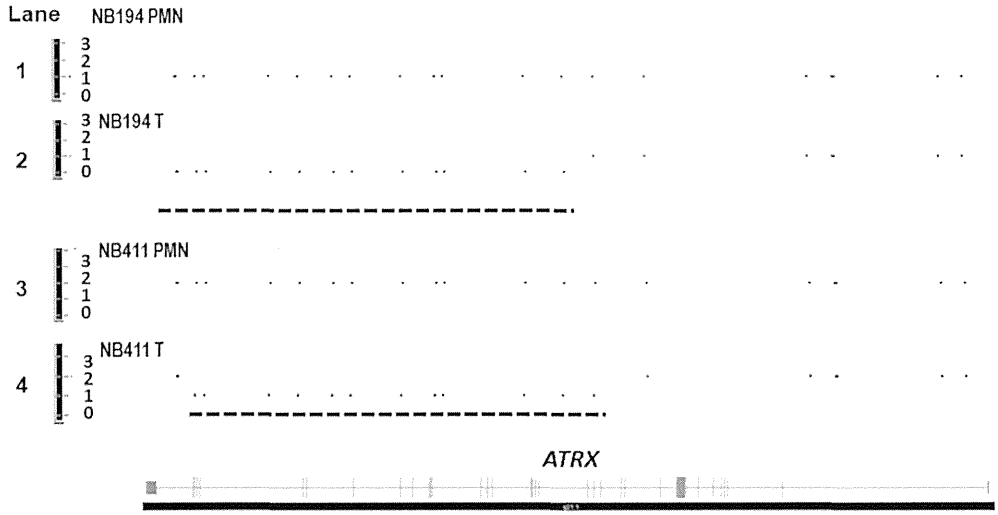

Fig. 1. Intensity of single nucleotide polymorphism (SNP) probes located in *ATRX* in neuroblastoma samples. Each dot indicates signal intensity of single nucleotide polymorphisms (SNPs) located in *ATRX* from an Affymetrix SNP 6.0 array. Since *ATRX* is located in chromosome X, male and female samples usually showed 1 and 2 copies in each SNP, respectively (lanes 1 and 3). Deleted loci were indicated by 0 and 1 copy in males and females, respectively (lanes 2 and 4). Solid lines show the prospective deleted lesions. A schematic of the intron–exon structure of *ATRX* is shown below, indicating the locations of exons are vertical lines.

3. Discussion

For immortalization in human tumor cells, telomerase is usually activated to maintain telomere length, which is shortened by cell division. However, in some tumor cells, a homologous recombination-based mechanism of telomere maintenance and elongation is activated [22] and this alternative lengthening of telomeres (ALT) is usually indicated by long telomeres [7,17]. High expression of telomerase activity correlates with advanced stages of disease and with tumor biological features that predict poor prognosis [7,23–25]. Indeed, tumors without detectable telomerase activity showed favorable outcomes except for some cases with elongated telomeres, suggesting the existence of ALT in NBLs [9].

Telomere maintenance by ALT also exists in unfavorable NBLs that were clinically suspected as chemo-resistant tumors without rapid growth [9]. Recently, identified *ATRX* or *DAXX* mutations in pancreatic neuroendocrine tumors and NBLs appeared to be loss-of-function mutations and thus, these mutations could lead to ALT activation [16].

In this study, we examined *ATRX* and *DAXX* alterations in the same cohort already analyzed for telomere biology [9]. Interestingly, all ALT activated NBLs had these alterations. Therefore, loss of function due to *ATRX* or *DAXX* alterations may contribute to ALT activation in NBLs, and it is possible that this is a direct effect of defects of histone H3.3 deposition at telomeres [26,27]. Although *ATRX* is located in chromosome X, both males and females were found to have *ATRX* mutations, consistent with previous work [10]. Additional studies will be required to determine the mechanism of ATRX function loss in both genders. Interestingly, an *ATRX* deleted infant case without long telomeres showed late recurrence regardless this case had been detected by screening. Although such cases are rare, NBLs with *ATRX* or *DAXX* alterations are a subgroup with high risk of late recurrence.

In our previous study for telomere biology in NBLs, clinical features of ALT-activating NBLs seemed to be markedly different from other NBLs [9]. These NBLs were clinically characterized as chemo-resistant tumors without rapid growth. Long telomeres in tumor cells might be disadvantageous for rapid growth. Therefore, cytotoxic therapy such as megachemotherapy with blood stem cell transplantation might be less effective in such NBLs. In such tumors with activated ALT due to *ATRX* or *DAXX* alterations, complete resection by surgery and careful attention for late recurrence should be performed to improve prognosis of these NBLs patients.

Recent advances in our understanding of NBL genetics and biology will greatly improve the outcome for patients with this complex heterogeneous disease [3,28]. Indeed, *MYCN* amplified NBLs [29], familial NBLs [30], *ALK* activated NBLs [31], and telomerase activated NBLs [7,32] have been identified and targeted molecular therapy for each of these NBLs

Table 1
Neuroblastoma cases with *ATRX* or *DAXX* aberrations.

	Age at diagnosis (mo.)/gender	Origin	INSS	*MYCN* (copies)	*DAXX/ATRX*	TRF (kb)	3'-OH	TRAP (TPG)	After CTx	Outcome
NBL003	73/M	retroperitoneal	4	1	Deletion	40	3.71	126.7	PR → PD	DOD (26 mo.)
NBL027	100/F	pelvic	4	200	Mut. (*DAXX*)	16	1.54	230.1	PD	DOD (27 mo.)
NBL094	23/M	adrenal	4	1	Mut. (*ATRX*)	26.1	2.96	9.28	SD → PD	DOD (52 mo.)
NBL194	129/M	adrenal	4	1	Deletion	28	3.85	6.16	PR → PD	DOD (42 mo.)
NBL225	42/M	adrenal	4	1	Deletion	31	1.71	4.6	PR → PD	DOD (53 mo.)
NBL292	40/F	retroperitoneal	4	1	Mut. (*ATRX*)	23	3.49	0.41	PR → PD	DOD (37 mo.)
NBL402	14/F	mediastinal	1	1	Mut. (*ATRX*)	15.6	3.31	7.31	-	NED (36 mo.)
NBL411	65/F	adrenal	4	1	Deletion	40	2.20	0.78	CR → PD	DOD (56 mo.)
NBL415	3/M	adrenal	4	1	Deletion	20.5	2.70	23.1	-	NED (127 mo.)
NBL418	8/F	adrenal	1	1	Deletion	20	3.05	5.22	-	NED (72 mo.)
NBL423	3/M	adrenal	2A	1	Deletion	17	2.39	42.3	-	NED (48 mo.)
NBL157*	8/M	adrenal	1	1	Deletion	12	1.72	11.12	CR → PD	DOD (25 mo.)

M: male, F: female, mo.: months of age, INSS: International Neuroblastoma Staging System, TRF: terminal restriction fragments, 3'-OH: 3'-overhang, TPG: Total Product Generated, Deletion: *ATRX* deletion, Mut: mutation, CTx: myeloablative chemotherapy, CR: complete remission, PR: partial remission, SD: stable disease, PD: progression of disease, DOD: dead of disease, NED: no evidence of disease.

* NB157 had *ATRX* deletion without elongated telomeres.

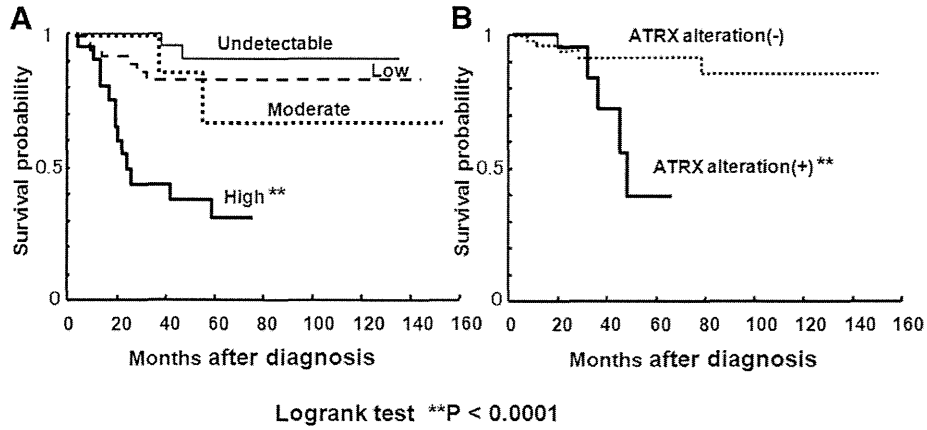

Fig. 2. Kaplan–Meier cumulative survival curves for patients with telomerase activity levels and ATRX alterations. A: Survival curves for patients with high, moderate, and low levels of telomerase activity in tumor samples. These data were analyzed in our previous report [9]. Patients with NBLs having high telomerase activity (n = 22, thick solid line) showed significantly poorer prognoses than those with moderate (n = 54) or low (n = 45) activity ($P < 0.001$). However, patients without high telomerase activity did not usually show good outcomes. B: Survival curve of patients with NBL tumors with *ATRX* mutation or deletion (n = 10) and that of the remaining patients without high telomerase activity (n = 88). The case with the *DAXX* mutation and the one *ATRX* deleted case were excluded in this analysis because these tumors had high telomerase activity. In NBLs without high telomerase activity, patients with altered *ATRX* tumors had significantly worse survival rates ($P < 0.001$). Length of follow-up in all cases was 69 ± 17 months (n = 121).

subgroups has now been attempted. *ATRX* or *DAXX* mutated NBLs might become a new subgroup for targeted molecular therapy.

Acknowledgments

This research was partially supported by Grant-in-Aids for Scientific Research (A) (No. 13313631 and 13370806) from the Ministry of Education, Culture, Sports, Science, and Technology and for Cancer Research by that (13801449) from theMinistry of Health, Labor, and Welfare of the Government of Japan.

We thank the Japanese pediatric oncologists and surgeons for providing tissue specimens and the clinical data of neuroblastoma patients under written informed consent.

References

[1] Hiyama E, Iehara T, Sugimoto T, et al. Effectiveness of screening for neuroblastoma at 6 months of age: a retrospective population-based cohort study. Lancet 2008;371:1173–80.
[2] Hiyama E, Hiyama K. Diagnostic and prognositic molecular markers in neuroblastoma. Kerala: Transworld Research Network; 2009 135–62.
[3] Pugh TJ, Morozova O, Attiyeh EF, et al. The genetic landscape of high-risk neuroblastoma. Nat Genet 2013;45:279–84.
[4] Deyell RJ, Attiyeh EF. Advances in the understanding of constitutional and somatic genomic alterations in neuroblastoma. Cancer Genet 2011;204:113–21.
[5] Mosse YP, Laudenslager M, Longo L, et al. Identification of ALK as a major familial neuroblastoma predisposition gene. Nature 2008;455:930–5.
[6] Trochet D, Bourdeaut F, Janoueix-Lerosey I, et al. Germline mutations of the paired-like homeobox 2B (PHOX2B) gene in neuroblastoma. Am J Hum Genet 2004;74:761–4.
[7] Hiyama E, Hiyama K, Yokoyama T, et al. Correlating telomerase activity levels with human neuroblastoma outcomes. Nat Med 1995;1:249–55.
[8] Hiyama E, Hiyama K, Shay JW, et al. Immunhistochemical detection of telomerase (hTERT) protein in human cancer tissues and a subset of cells in normal tissues. Neoplasia 2001;3:17–26.
[9] Onitake Y, Hiyama E, Kamei N, et al. Telomere biology in neuroblastoma: telomere binding proteins and alternative strengthening of telomeres. J Pediatr Surg 2009;44:2258–66.
[10] Cheung NK, Zhang J, Lu C, et al. Association of age at diagnosis and genetic mutations in patients with neuroblastoma. JAMA 2012;307:1062–71.
[11] Brodeur GM, Pritchard J, Berthold F, et al. Revisions of the international criteria for neuroblastoma diagnosis, staging, and response to treatment [see comments]. J Clin Oncol 1993;11:1466–77.
[12] Shimada H, Ambros IM, Dehner LP, et al. The International Neuroblastoma Pathology Classification (the Shimada system). Cancer 1999;86:364–72.
[13] Sawaguchi S, Kaneko M, Uchino J, et al. Treatment of advanced neuroblastoma with emphasis on intensive induction chemotherapy: a report from the Study Group of Japan. Cancer 1990;66:1879–87.
[14] Yuan E, Haghighi F, White S, et al. A single nucleotide polymorphism chip-based method for combined genetic and epigenetic profiling: validation in decitabine therapy and tumor/normal comparisons. Cancer Res 2006;66:3443–51.
[15] Zhang J, Benavente CA, McEvoy J, et al. A novel retinoblastoma therapy from genomic and epigenetic analyses. Nature 2012;481:329–34.
[16] Heaphy CM, de Wilde RF, Jiao Y, et al. Altered telomeres in tumors with ATRX and DAXX mutations. Science 2011;333:425.
[17] Hiyama E, Yokoyama T, Hiyama K, et al. Alteration of telomeric repeat length in adult and childhood solid neoplasias. Int J Oncol 1995;6:13–6.
[18] Hashimoto M, Kyo S, Masutomi K, et al. Analysis of telomeric single-strand overhang length in human endometrial cancers. FEBS Lett 2005;579:2959–64.
[19] Stewart SA, Ben-Porath I, Carey VJ, et al. Erosion of the telomeric single-strand overhang at replicative senescence. Nat Genet 2003;33:492–6.
[20] Kim NW, Piatyszek MA, Prowse KR, et al. Specific association of human telomerase activity with immortal cells and cancer. Science 1994;266:2011–5.
[21] Piatyszek MA, Kim NW, Weinrich SL, et al. Detection of telomerase activity in human cells and tumors by a telomeric repeat amplification protocol (TRAP). Methods Cell Sci 1995;17:1–15.
[22] Hiyama E, Yamaoka H, Kondo S, et al. Heterogeneous subgroups in human neuroblastoma for clinically relevant risk stratification. Pediatr Surg Int 2007;23:1051–8.
[23] Hiyama E, Hiyama K, Ohtsu K, et al. Telomerase activity in neuroblastoma: is it a prognostic indicator of clinical behavior? Eur J Cancer 1997;33:1932–6.
[24] Reynolds CP, Zuo JJ, Hong CM, et al. Telomerase RNA expression in neuroblastoma correlates with high stage and clinical outcome. Proc A Assoc Cancer Res 1996;37:199.
[25] Hiyama E, Hiyama K, Yokoyama T, et al. Length of telomeric repeats in neuroblastoma: correlation with prognosis and other biological characteristics. Jpn J Cancer Res 1992;83:159–64.
[26] Lovejoy CA, Li W, Reisenweber S, et al. Loss of ATRX, genome instability, and an altered DNA damage response are hallmarks of the alternative lengthening of telomeres pathway. PLoS Genet 2012;8:e1002772.
[27] Bower K, Napier CE, Cole SL, et al. Loss of wild-type ATRX expression in somatic cell hybrids segregates with activation of Alternative Lengthening of Telomeres. PLoS One 2012;7:e50062.
[28] Sridhar S, Al-Moallem B, Kamal H, et al. New insights into the genetics of neuroblastoma. Mol Diagn Ther 2013;17:63–9.
[29] Brodeur GM, Seeger RC, Schwab M, et al. Amplification of N-myc in untreated human neuroblastoma correlated with advanced stage. Science 1984;224:1121–4.
[30] Wylie L, Philpott A. Neuroblastoma progress on many fronts: the Neuroblastoma Research Symposium. Pediatr Blood Cancer 2012;58:649–51.
[31] Ogura T, Hiyama E, Kamei N, et al. Clinical feature of anaplastic lymphoma kinase-mutated neuroblastoma. J Pediatr Surg 2012;47:1789–96.
[32] Hiyama E, Hiyama K. Molecular and biological heterogeneity in neuroblastoma. Curr Genomics 2005;6:319–32.

Genes to Cells

FAST-id system for enrichment of cells with TALEN-induced mutations and large deletions

Daisuke Tokumasu[1†], Tetsushi Sakuma[1†], Yoko Hayashi[2], Sayaka Hosoi[1], Eiso Hiyama[2] and Takashi Yamamoto[1*]

[1]*Department of Mathematical and Life Sciences, Graduate School of Science, Hiroshima University, 1-3-1 Kagamiyama, Higashi-Hiroshima, Hiroshima 739-8526, Japan*
[2]*Natural Science Center for Basic Research and Development (N-BARD), Hiroshima University, 1-2-3 Kasumi, Minami-ku, Hiroshima 734-8551, Japan*

Transcription activator-like effector nuclease (TALEN)-mediated genome editing is a powerful technique for analyzing gene functions in various cells and organisms. At target loci, TALENs can not only introduce short insertions and deletions, but also yield large deletions through the use of two TALEN pairs. Here, we report easy and efficient methods for enrichment of cells with TALEN-induced mutations and large deletions. First, we established the fluorescence-activated sorting of TALEN-induced deletions (FAST-id) system that enabled fluorescence-activated cell sorting-mediated enrichment of cells with TALEN-induced mutations. In the FAST-id system, either EGFP or mCherry and TALENs were co-expressed. Using dual fluorescence selection, both left and right TALEN-expressing cells were easily concentrated, resulting in enrichment of TALEN-mediated mutated cells. Next, to apply the FAST-id system to enrichment of cells with large deletions, we developed the fast unification of separate endonucleases (FUSE) method for assembly of two TALENs into a single expression vector. Using the FUSE method, we easily obtained a TALEN pair-expressing plasmid driven by a single promoter. By combining the FAST-id system and FUSE method, cells with large deletions were efficiently enriched. To the best of our knowledge, this is the first report of enrichment of cells with TALEN-induced large deletions.

Introduction

Recently, targeted genome engineering using engineered nucleases, including zinc finger nucleases (ZFNs) and transcription activator-like effector nucleases (TALENs), has attracted attention as an effective tool in various cultured cells or organisms (Urnov *et al.* 2010; Joung & Sander 2013). Engineered nucleases are composed of a sequence-specific DNA-binding domain and a nonspecific DNA cleavage domain derived from the FokI restriction endonuclease, which can induce double-strand breaks (DSBs) into target sequences. Engineered nuclease-induced DSBs can be repaired by nonhomologous end-joining (NHEJ) or homology-directed repair (HDR). Error-prone NHEJ repair frequently leads to the introduction of short insertions and deletions (indels), frequently resulting in gene disruption via a frameshift (Santiago *et al.* 2008). In the template-dependent repair pathway, HDR, insertion of exogenous genes into the genome is achieved using a donor template containing ~1-kb homology arms adjacent to the target sequence (Moehle *et al.* 2007; Hockemeyer *et al.* 2011). Furthermore, DSBs can be introduced into two sites through the use of two pairs of ZFNs or TALENs, resulting in chromosomal deletions, inversions, and duplications when two DSB sites are on the same chromosome (Lee *et al.*

Communicated by: Masayuki Miura
**Correspondence:* tybig@hiroshima-u.ac.jp
†These authors contributed equally to this study.

DOI: 10.1111/gtc.12142

2010, 2012) and chromosomal translocations when the sites are on different chromosomes (Brunet *et al.* 2009; Piganeau *et al.* 2013).

To facilitate the use of TALEN technology, it is absolutely necessary to develop easy and efficient methods for selecting TALEN-induced mutated cells. Currently, several methods have been reported for enrichment of ZFN- or TALEN-induced mutated cells. A surrogate reporter system (Kim *et al.* 2011, 2013a) can be used to validate the activity of ZFNs or TALENs in living cells and to select potentially mutated cells by sorting based on fluorescence intensity, magnetic separation, or antibiotic selection. As another method, enrichment of TALEN-induced mutated cells by co-expressing TALENs and fluorescent proteins and subsequent sorting of TALEN-expressing cells based on fluorescence intensity was reported (Ding *et al.* 2013). However, there are no reports regarding methods for enrichment of chromosomally rearranged cells using two TALEN pairs.

Here, we report efficient methods for enrichment of cells with TALEN-induced mutations and chromosomal deletions. We constructed vectors to visualize the expression levels of TALENs on the basis of fluorescence intensity. Subsequently, we showed that sorting of cells exhibiting high expression of TALENs based on fluorescence intensity using fluorescence-activated cell sorting (FACS) enabled enrichment of cells with TALEN-induced mutations or large deletions.

Results

Enrichment of cells with TALEN-induced mutations by FACS

To select cells in which mutations such as indels are introduced into the target sites by TALENs, it is necessary to distinguish cells showing high expression of both left and right TALENs from a variety of cells expressing either the left or right TALEN alone or neither TALEN. To monitor the expression of a TALEN pair, we planned to construct two types of plasmid vectors in which a gene for a fluorescent protein (mCherry or EGFP) was bicistronically linked to a gene for one TALEN (L or R) via the 'self-cleaving' 2A peptide sequence (Fig. 1A). Following transfection of these plasmids into mammalian cells, it was expected that both the TALEN and the fluorescent protein would be expressed as separate proteins. Therefore, by sorting of positive cells for both mCherry and EGFP fluorescence, we can easily select

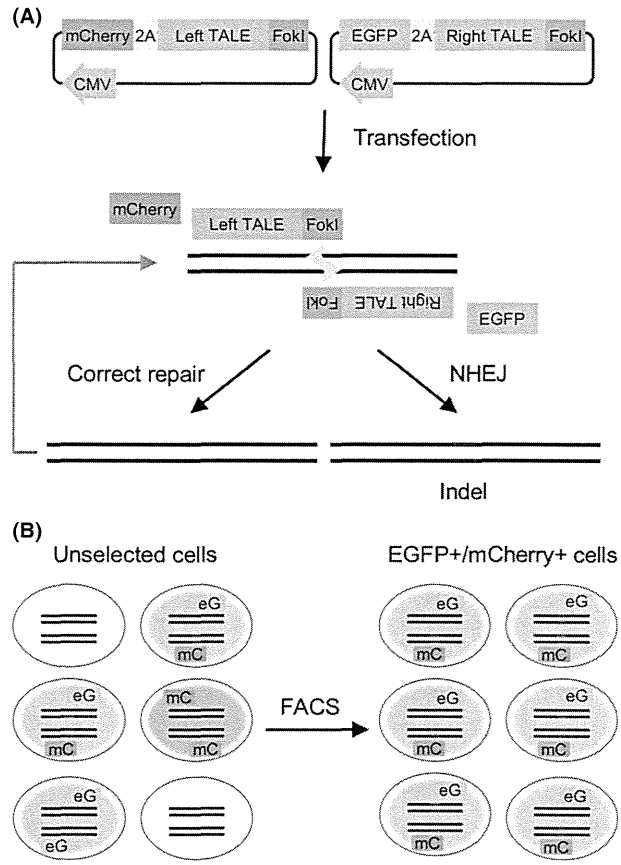

Figure 1 Schematic overview of the fluorescence-activated sorting of TALEN-induced deletions (FAST-id system). (A) Scheme of TALEN-mediated mutagenesis using the FAST-id system. A TALEN and either EGFP or mCherry are co-expressed and translated as individual proteins, which allows visualization of the expression level of the TALEN by the fluorescence intensity. The NHEJ pathway often introduces insertions and/or deletions (indels, red lines) at the TALEN target site. CMV, cytomegalovirus promoter; 2A, 2A sequence. (B) Scheme of enrichment of cells with TALEN-induced mutations. Fluorescence intensity-dependent cell sorting using fluorescence-activated cell sorting enables selection of cells showing high expression of both the left and right TALENs, resulting in enrichment of cells with TALEN-induced mutations. eG, EGFP; mC, mCherry.

cells expressing both the left and right TALENs, which are expected to introduce indel mutations at the target site (Fig. 1B). We referred to this system as the 'fluorescence-activated sorting of TALEN-induced deletions (FAST-id)' system.

To investigate whether cells with TALEN-induced mutations can be efficiently enriched by the FAST-id system, we constructed fluorescent protein-2A-TALEN plasmids targeting the human hypoxanthine

phosphoribosyltransferase 1 (*HPRT1*) locus (*HPRT1*_B TALEN), transfected these plasmids into HCT116 cells, and performed flow cytometric analyses. *HPRT1* is an X-linked gene, and HCT116 cells have only one copy of this gene in their genome. As shown in Fig. 2A, the transfected cells showed various intensities of EGFP and mCherry fluorescence, indicating that there were variations in the TALEN expression levels in the transfected cells (Fig. 2A, left panel). To evaluate the extent of the TALEN-induced mutations, we carried out PCR amplification of the target region of the *HPRT1*_B TALEN using genomic DNA extracted from unselected cells and EGFP−/mCherry− and EGFP+/mCherry+ cells (Fig. 2A, squares), and examined each mutation rate by restriction fragment length polymorphism (RFLP) analysis after digestion with the restriction enzyme Hpy188I, which has a site located in the middle of the *HPRT1*_B TALEN spacer region. If a mutation was introduced into the

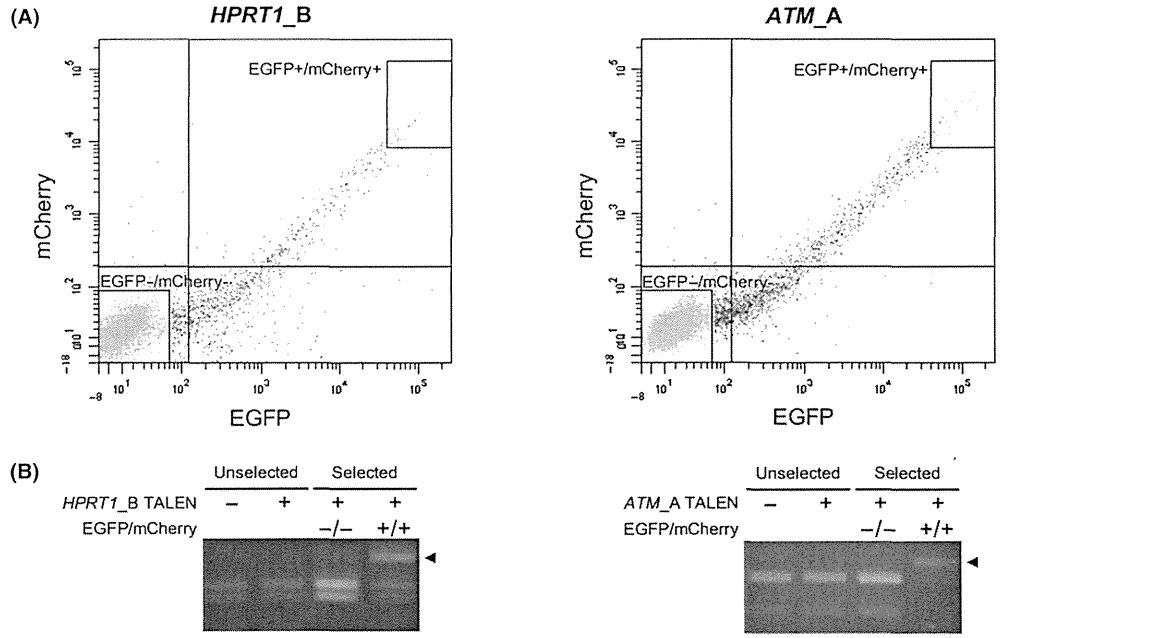

(C)

*HPRT1*_B Unselected cells 20%(3/15)

```
agtgatagatCCATTCCTATGACTGTAGATtttatcagactgaagAGCTATTGTGTGAGTATatttaatata WT
agtgatagatCCATTCCTATGACTGTAGATttctat----cacagAGCTATTGTGTGAGTATatttaatata
agtgatagatCCATTCCTATGACTGTAGATtttatcagactggagAGCTATTGTGTGAGTATatttaatata
agtgatagatCCATTCCTATGACTGTAGATtttatcagactgaagAGCTgTTGTGTGAGTATatttaatata
```

*HPRT1*_B EGFP+/mCherry+ cells 83%(10/12)

```
agtgatagatCCATTCCTATGACTGTAGATtttatcagactgaagAGCTATTGTGTGAGTATatttaatata WT
agtgatagatCCATTCCTATGACTGTAGATtttat---actgaagAGCTATTGTGTGAGTATatttaatata x2
agtgatagatCCATTCCTATGACTGTAGATttta-------gaagAGCTATTGTGTGAGTATatttaatata x2
agtga----------------------------------------------------------ta x2
agtgatagatCCATTCCTATGACTGTAGATtttatc------aagAGCTATTGTGTGAGTATatttaatata
agtgatagatCCATTCCTATGACTGTAGATtttatc-------agAGCTATTGTGTGAGTATatttaatata
agtgatagatCCATTCCTATGACT---------------tgaagAGCTATTGTGTGAGTATatttaatata
agtgatagatCCATTCCTATGAC----------------tgaagAGCTATTGTGTGAGTATatttaatata
```

*ATM*_A Unselected cells 20%(3/15)

```
aaccatgagtCTAGTACTTAATGATCtgcttatctgctgccGTCAACTAGAACATGATagagctacag WT
aaccatgagtCTAGTACTTAATGAT----------ctgccGTCAACTAGAACATGATagagctacag
aaccatgagtCTAGTACTTgATGATCtgcttatctgctgccGTCAACTAGAACATGATagagctacag
aaccatgagtCTAGTACTTAAcGATCtgcttatctgctgccGTCAACTAGAACATGATagagctacag
```

*ATM*_A EGFP+/mCherry+ cells 100%(14/14)

```
aaccatgagtCTAGTACTTAATGATCtgcttatctgctgccGTCAACTAGAACATGATagagctacag WT
aaccatgagtCTAGTACTTAATGATCtgctta------gccGTCAACTAGAACATGATagagctacag x4
aac--------------------------------------CTAGAACATGATagagctacag x4
aaccatgagtCTAGTACTTAATGATC----------------AACTAGAACATGATagagctacag x4
---------------------------------------AACTAGAACATGATagagctacag -185
aaccatgagtCTAGTACTTAATGATCtgctta-----tgccGTCAACTAGAACATGATagagctacag
```

Figure 2 Enrichment of cells with TALEN-induced mutations. (A) Flow cytometric analyses of HCT116 cells transfected with *HPRT1*_B (left panel) or *ATM*_A (right panel) TALEN-encoding plasmids. Cells showing high expression (EGFP+/mCherry+) and minimal expression (EGFP−/mCherry−) were collected (squares). Indexes of numbers and percentages of collected cells are listed in Table S5 in Supporting Information. Vertical and horizontal lines indicate background fluorescence levels of EGFP and mCherry, respectively. (B) RFLP analyses of mutations induced by *HPRT1*_B (left panel) or *ATM*_A (right panel) TALENs. The genomic PCR products of unselected, EGFP−/mCherry−, and EGFP+/mCherry+ cells transfected with the *HPRT1*_B or *ATM*_A TALEN-encoding plasmids or untransfected cells were purified, digested, and analyzed by agarose gel electrophoresis. The arrowheads indicate the expected positions of the undigested products. (C) Sequences observed in unselected and EGFP+/mCherry+ cells transfected with the *HPRT1*_B or *ATM*_A TALEN-encoding plasmids. The wild-type sequence of *ATM* or *HPRT1* is shown at the top with the TALEN target sequence (capital letters with underlines). Deletions are indicated by dashes.

spacer region of the *HPRT1*_B TALEN target site, mutated alleles would be detected as resistant fragments against Hpy188I digestion. As shown in Fig. 2B, an Hpy188I-resistant fragment was strongly detected in the PCR products from EGFP+/mCherry+ cells, but scarcely detected among the PCR products from unselected cells and EGFP−/mCherry− cells (Fig. 2B, left panel). Similarly, we constructed fluorescent protein-2A-TALEN plasmids targeting the ataxia–telangiectasia mutated (*ATM*) locus (*ATM*_A TALEN). *ATM* is an autosomal gene, and HCT116 cells have two copies of this gene in the genome. After transfection of these plasmids and fluorescence-mediated cell sorting (Fig. 2A, right panel), we carried out RFLP analysis with the restriction enzyme Fnu4HI. Consistent with the results for the *HPRT1* gene, a restriction enzyme-resistant fragment was observed in the PCR products from EGFP+/mCherry+ cells, but hardly observed among the PCR products from unselected and EGFP−/mCherry− cells (Fig. 2B, right panel).

Next, to investigate the rate and context of the mutations, we analyzed the mutations introduced into the target sites by the TALENs. DNA fragments amplified by PCR using genomic DNA extracted from unselected or EGFP+/mCherry+ cells were subcloned, and their nucleotide sequences were determined (Fig. 2C). We found that the mutation frequency of the *HPRT1*_B TALEN target site in EGFP+/mCherry+ cells was 83%, whereas that in unselected cells was 20%, showing 4.2-fold enrichment of cells with TALEN-induced mutations (Table 1). Similarly, in the fluorescent protein-2A-*ATM*_A TALEN plasmid-transfected cells, the mutation frequency in EGFP+/mCherry+ cells was 100%, whereas that in unselected cells was 20%, showing 5-fold enrichment of cells with indel mutations (Table 1). These results suggest that the FAST-id system is efficient for enrichment of cells with TALEN-mediated mutations.

Establishment of a unification system for TALEN expression vectors

Although systems for enrichment of cells with TALEN-induced indel mutations have been reported (Kim *et al.* 2011, 2013a; Ding *et al.* 2013), there are no previous reports regarding systems for enrichment of cells with TALEN-mediated chromosomal deletions. For TALEN-mediated chromosomal deletions, it is necessary to express two pairs of TALENs in cells to cut two different sites on the same chromosome. To monitor the expression levels of the two pairs of TALENs and select cells using the FAST-id system, the expression of four kinds of fluorescent proteins would be required. However, it is thought that the transfection efficiency of four types of fluorescent protein-2A-TALEN plasmids may be low. In addition, it is difficult to sort cells expressing two pairs of TALENs on the basis of four kinds of fluorescence intensity, because the fluorescence spectra must overlap. Therefore, we planned to construct a vector expressing a fluorescent protein and a pair of TALENs in a single plasmid to allow monitoring of the expression of the TALEN pair by a single fluorescent protein, such that we can select cells showing high expression of two pairs of TALENs using only two fluorescent proteins.

To realize the above-described system, we established the 'fast unification of separate endonucleases (FUSE)' method. In the FUSE method, we construct left and right TALEN expression vectors as separate vectors at the first step, and subsequently unify these vectors into a single expression vector by digestion and ligation at the second step (Fig. 3A). In the left TALEN expression vector, a fluorescent protein gene is ligated to the left TALEN gene via the 2A sequence, whereas in the right TALEN expression vector, the 2A sequence is inserted in the upstream of the right TALEN gene. Furthermore, BamHI sites are inserted in the upstream of the stop codon of the

Table 1 Comparison of mutation frequencies in unselected and EGFP+/mCherry+ cells

	Mutation frequency (%)			
TALEN	Unselected	EGFP+/mCherry+	Fold enrichment	Types of mutation
*HPRT1*_B	20	83	4.2	Indel
*ATM*_A	20	100	5.0	Indel
*HPRT1*_B + *HPRT1*_E	3	41	13.7	Chromosomal deletion
*ATM*_A + *ATM*_D	11	77	7.0	Chromosomal deletion

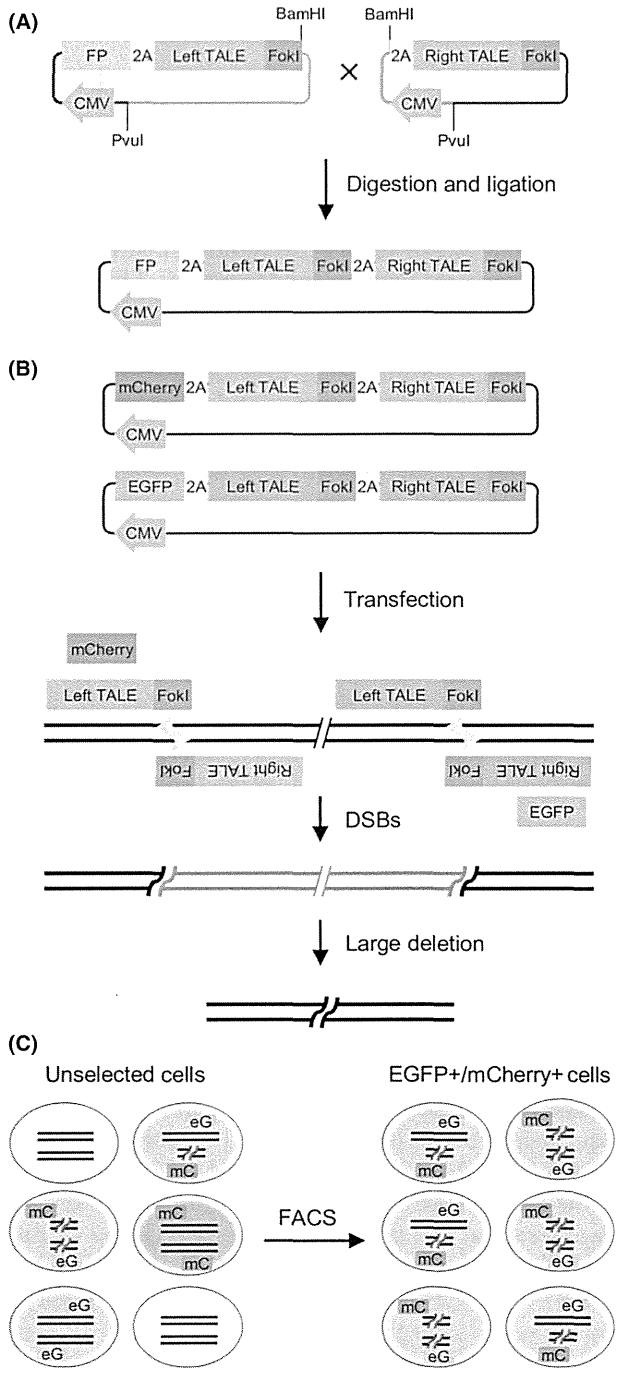

Figure 3 Schematic overview of the combined system using the fast unification of separate endonucleases (FUSE) method and fluorescence-activated sorting of TALEN-induced deletions (FAST-id) system. (A) Scheme of the FUSE method. Left and right TALEN expression vectors are constructed separately and subsequently unified by double digestion with BamHI and PvuI followed by ligation. FP, fluorescent protein. (B) Scheme for combining the FUSE method and FAST-id system. Transfection of two kinds of one TALEN pair-encoding plasmids created by the FUSE method into cells enables the introduction of two double-strand breaks on the target chromosome, resulting in the introduction of a large deletion. (C) Scheme of enrichment of chromosomally deleted cells. Fluorescence intensity-dependent cell sorting using fluorescence-activated cell sorting enables selection of cells showing high expression of the two TALEN pairs, resulting in enrichment of cells with the chromosomal deletion.

left TALEN gene and between the start codon and the 2A sequence in the right TALEN expression vector for the assembly of both TALENs. Importantly, we can evaluate the activity of these TALEN expression vectors by a single-strand annealing (SSA) assay (Sakuma *et al.* 2013), because they retain the structure of a TALEN expression vector. A pair of TALENs, whose activity is confirmed, can be unified quickly by BamHI digestion and ligation along with removal of unnecessary start and stop codons to form a single gene encoding fluorescent protein-2A-left TALEN-2A-right TALEN. Although the footprint of the BamHI site (5′-GGATCC-3′) is retained in front of the 2A-right TALEN, it functions as part of a GSG linker at the N-terminus of the 2A peptide. Thus, we can enable seamless ligation of the left and right TALEN array into a single expression vector (Fig. 3A) to efficiently obtain cells with two DSB-induced large deletions (Fig. 3B).

Enrichment of cells with TALEN-induced large deletions using the FUSE method and FAST-id system

Next, we carried out the enrichment of chromosomally deleted cells by combining the FUSE method and FAST-id system (Fig. 3C). We planned to construct two pairs of TALENs targeting different regions of the *HPRT1* locus (*HPRT1*_B and *HPRT1*_E, Fig. 4A). After confirming the mutagenic frequency using separate TALEN expression vectors by the SSA assay, we used the FUSE method to unify the *HPRT1*_B TALEN pair into a single expression vector containing the mCherry sequence and the *HPRT1*_E TALEN pair targeting approximately 1100-bp upstream of the *HPRT1*_B TALEN target site into a single expression vector containing the EGFP sequence. We then examined the mutagenic frequencies of the *HPRT1*_B and *HPRT1*_E TALENs as single expression vectors or separate

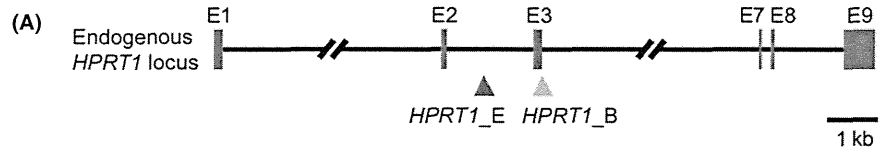

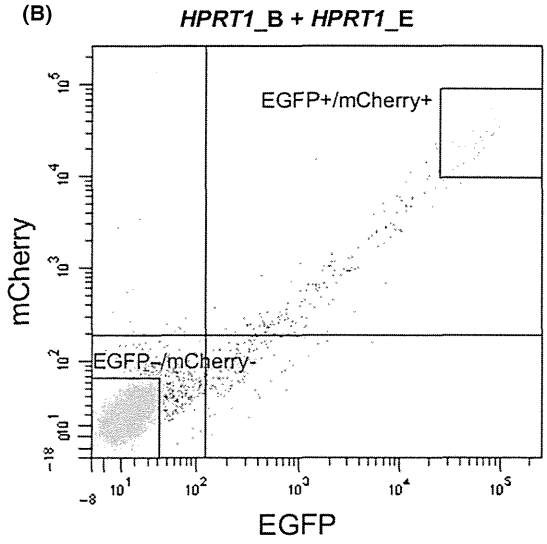

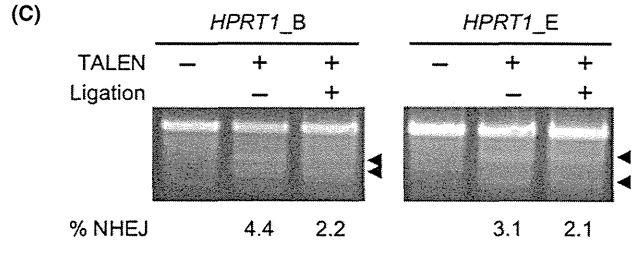

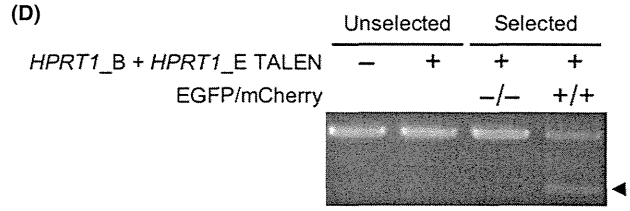

(E) *HPRT1*_B + *HPRT1*_E TALEN (Unselected cells)

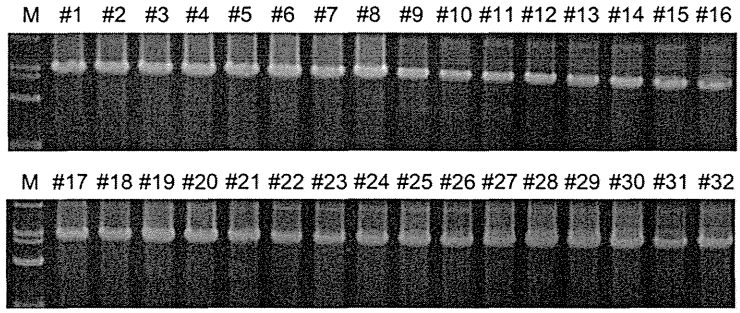

***HPRT1*_B + *HPRT1*_E Unselected cells** 3%(1/36)

```
       HPRT1_E TALEN Left site                                  HPRT1_B TALEN Right site
agcattctgtCTTATGGAGATACCATAactgatttaaccagt..1139bp..tttatcagactgaagAGCTATTGTGTGAGTATatttaatata WT
agcattctgtCTTATGGAGATACCATAactg-ttt-----------------------actgaagAGCTATTGTGTGAGTATatttaatata
```

(F) *HPRT1*_B + *HPRT1*_E TALEN (EGFP+/mCherry+ cells)

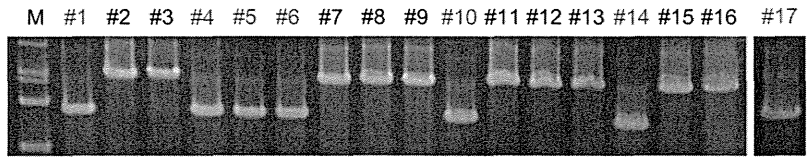

***HPRT1*_B + *HPRT1*_E EGFP+/mCherry+ cells** 41%(7/17)

```
       HPRT1_E TALEN Left site                                  HPRT1_B TALEN Right site
agcattctgtCTTATGGAGATACCATAactgatttaaccagt..1139bp..tttatcagactgaagAGCTATTGTGTGAGTATatttaatata WT
agcattctgtCTTATGGAGATACCATAactga-------------------------------aagAGCTATTGTGTGAGTATatttaatata x2
agcattctgtCTTATGGAGATACCATAactga-------------------------------agAGCTATTGTGTGAGTATatttaatata x2
agcattctgtCTTATGGAGATACCATAactga---------------------------------gAGCTATTGTGTGAGTATatttaatata
agcattctgtCTTATGGAGATACCATAactgaat-----------------------------aagAGCTATTGTGTGAGTATatttaatata
agcattctgtCTTATGGAGATACCA---ctgat-----------------------------aagAGCTATTGTGTGAGTATatttaatata
```